Dear Editor and Reviewers,

Thank you for your detailed comments and suggestions about our manuscript entitled “A high frequency and high resolution image time series of the Gornergletscher – Swiss Alps – derived from repeated UAV surveys”.

The manuscript has been revised accordingly. Please find hereafter an item-by-item response to your comments.

Hoping that our responses answer your concerns, and that our propositions of improvements will fulfil your expectations,

Best regards,

Lionel Benoit, on behalf of all co-authors.

Responses to the comments of Reviewer #1:

In the following point-by-point reply, RC denotes a reviewer comment and AR denotes our response to the comment.

RC: The first concern is based on the relative geo-referencing, the authors have chosen not to use real ground control points. While they have chosen one common bundle-adjustment as master, to "stitch" other control against it. It is common in photogrammetry to distribute GCP’s and have them placed especially at the outer ends. This reduces "banana" bending, caused by imperfections in the lens model. However, this is not done in this study, thus one can assume such effects are here at hand as well. I am well aware of the logistics within such terrain, thus I am not asking to do this procedure. Nevertheless, I propose the authors put a bit more emphasis into describing the potential errors associated with this effect/shortcoming. I hope if this is done rightfully, it will reduce the mistake of over interpretation by other users of this data.

AR: The impact of the absence of GCPs during the master bundle adjustment is now discussed in a new paragraph at the end of the section 3.1 ‘generation of co-registered orthomosaics and DEMs’ (p6 – l 1-20). In this new paragraph we mention the possible existence of internal deformations and we describe in detail the impact of the absence of GCPs on geo-referencing.
In addition, the actual amplitude of the internal deformations is now assessed by studying the residuals of the co-registration of the orthomosaic derived from the master bundle adjustment with respect to an orthomosaic produced by the Swiss mapping agency. The amplitude of these deformations is shown to be small, and discussed in details at the end of the section 4.1 dedicated to the quality assessment of the orthomosaics (p 9, l15-22 -> p10, l 1-7). In addition, the residuals of the co-registration procedure are now displayed in the revised Fig 4.

RC: My second concern is focused around the matching maps, which are less standard products, and therefore implementation details need to be discussed more. Although not standard, there do exist best-practices, and because the authors deviate from this I highlight some steps which may need more clarification, or adjustments, in order to improve the resulting matching map product or get a better understanding why certain steps are taken.

AR: To better explain the generation of the Matching Maps, we fully revised the section '3.2: Surface displacement tracking: generation of Matching Maps' (in particular p 6, l 20 -> p 7, l 20). When re-writing this section, we followed three guidelines:
- Clearly state that Matching Maps are nothing but displacement maps.
- Contextualize our procedure with respect to well established software, highlighting similarities and differences.
- Benchmark our Matching Map Maker utility with two well-established tools dedicated to displacement calculation by image correlation (we chose CIAS - https://www.mn.uio.no/geo/english/research/projects/icemass/cias/ and Imcorr - https://nsidc.org/data/velmap/imcorr.html as benchmarks). The results of these tests have been added to a sub-repository of the MMM source code, which is mentioned in the main manuscript (P7, L14-18).

RC: The similarity score is "maximum absolute error" on grayscale images. This is a peculiar choice as throughout the season and throughout the day the sun has changing illumination directions. Though this similarity measure is very sensitive towards such effects. Commonly, the normalized cross correlation is used […].

AR: The choice of MAE as similarity score is now motivated in the manuscript and contextualized with references (p7, l3-5). In addition, the impact of illumination effects on MAE is now discussed in details (p7, l5-9).
To ensure that the use of MAE as similarity score does not impair the results of the matching procedure, we compared MAE with other similarity scores, namely: (1) the normalized cross-correlation and (2) a high-pass filter (cutting wavelength=25m) coupled with a cross correlation (similar to (Fahnestock et al, 2016)). The results below, also reported in a sub-repository of the MMM source code and mentioned in the manuscript (p13, l11-12), show that MAE performs as good as a high-pass filter (cutting wavelength=25m) coupled with a cross-correlation, and outperforms the normalized cross-correlation.

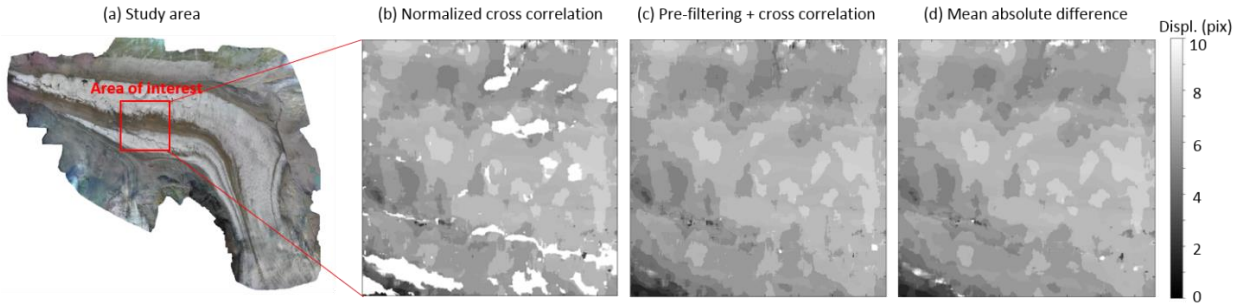

Figure: Surface displacements (July 13th – July 26th) estimated by feature tracking using different similarity scores. (a) Situation map. (b) Displacements estimated by maximum normalized cross-correlation. (c) Displacements estimated by high pass filtering (cutting wavelength = 25 m) and maximum cross-correlation. (d) Displacements estimated by minimum of the mean absolute differences. In (b-d), all parameters of the tracking algorithm besides the similarity score are the same for the three scenarios (search template 21 x 21 pixels, search window 400 x 400 pixels).

RC: […] the images are either pre-filtered with a high-pass-filter [Fahnestock 2016] or a Wallis-filter [Dehecq 2018]. I expect this will improve the results considerable.

AR: A first reason to pre-filter the images is the improvement of the normalization factor when the cross-correlation is used as similarity score. This is clearly visible in the results of the previous test assessing different similarity scores. But when mean absolute differences are used (as is the case in our manuscript), no normalization is required, and there is therefore no need for pre-filtering to help normalizing the similarity score.
Another argument for using pre-filtering is to focus on features with a characteristic scale close to the resolution of the images. We think that such use of pre-filtering is mostly relevant in case of matching satellite images with meter-scale resolution or coarser. In our case (10 cm resolution) a high-pass-filter with a cutting wavelength close to the resolution of the images extracts very small features such as small superficial cracks, shadows or snow patches, which are probably not very persistent in time and thus not relevant to track. Instead, we prefer to use the full information of the patch of interest (5m x 5m) that also includes larger and more persistent features.

RC: Also the use of orientation-correlation [Heid 2012] or COSI-CORR [leprince 2007] might be a more robust procedure.

AR: To ensure that our Matching Map Maker utility is reliable, we benchmarked it by comparison with velocity maps calculated using the well-established CIAS and Imcorr algorithms. The results below show that our method does not introduce bias nor inconsistencies. To reassure the user about the reliability of our utility, we added the figures below in a sub-directory of the repository of the Matching Map Maker utility. In addition, we mention the existence of these tests (and the associated results) in the manuscript (p7, l16-18 and p13, l7-13).

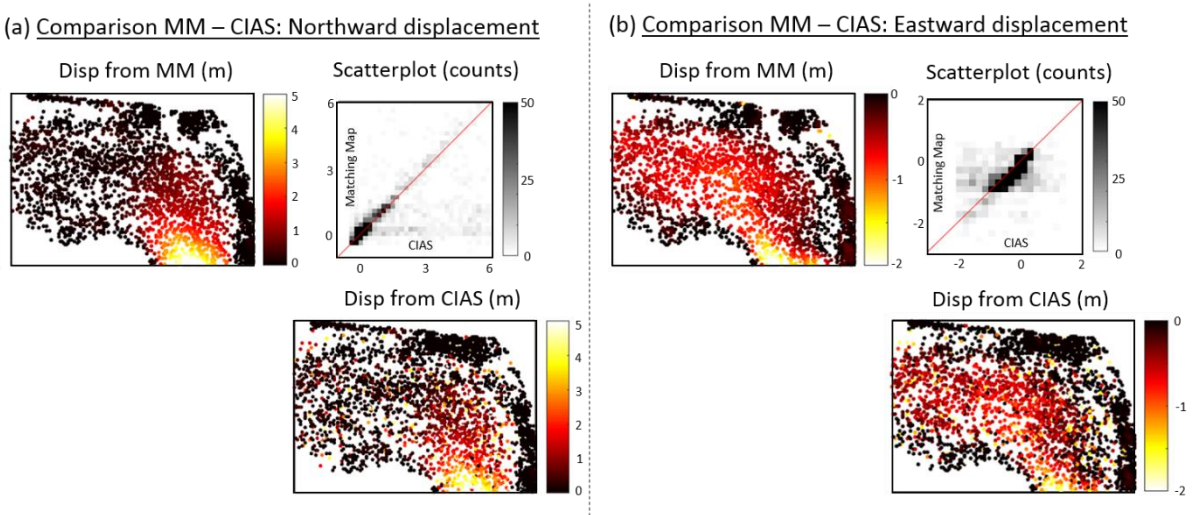

Figure: Comparison of estimated displacements derived from the Matching map (top plots) and from the CIAS software (bottom plots). Period of interest: July 13th – July 26th. (a) Northward displacement, (b) Eastward displacement. The only noticeable differences are due to residual noise in the CIAS results due to the simple set up we applied.

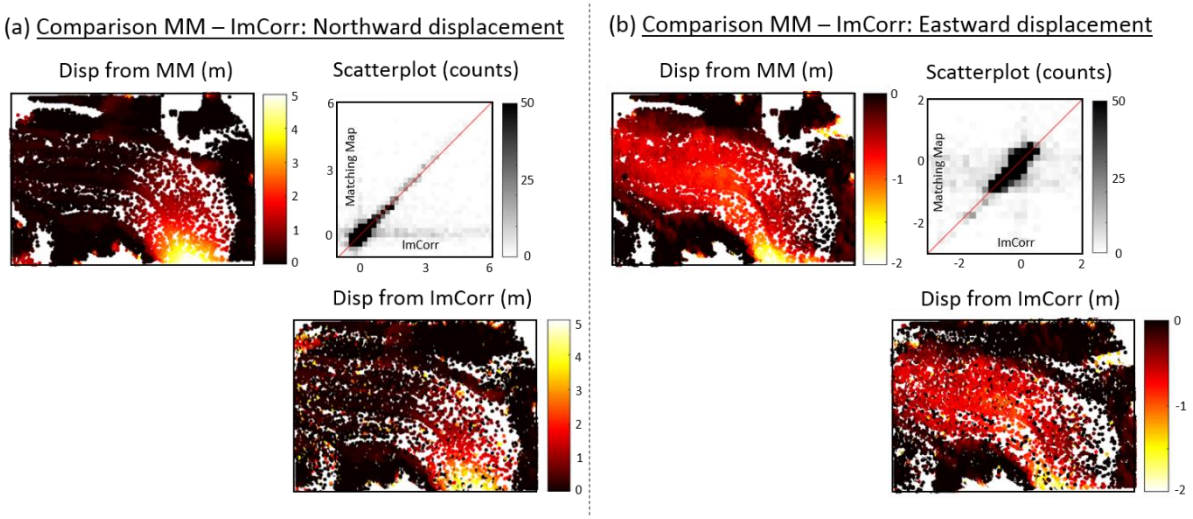

Figure: Comparison of estimated displacements derived from the Matching map (top plots) and from the ImCorr software (bottom plots). Period of interest: July 13th – July 26th. (a) Northward displacement, (b) Eastward displacement. The only noticeable differences are due to residual noise in the ImCorr results due to the simple set up we applied.

RC: The matching maps seem to have an integer displacement, and no sub pixel localization is applied. While these procedures are able to increase the precision considerably.

AR: We think that sub-pixel localization is mostly useful when the amplitude of the displacement between two dates is small with regard to the resolution of the images. This is the case for instance when glacier velocity is derived from satellite images, or when satellite images are used to measure ground deformations induced by tectonics (typical application of COSI-corr). However, in our case, the resolution of the ortho-images used to compute the matching maps is high (10cm) compared to the expected displacement of the glacier (20-50cm/day => 2.8-7m displacement in two weeks). We therefore think that the absence of sub-pixel localization in our procedure is not a major issue.

RC: The spacing of velocity product is at pixel level, though in products like GoLIVE for example, the spacing of the grid is as large as the template size (in this case 300 meters). Similar processing in SAR speckle tracking is done with only 50% overlap [van wychen 2018]. This is done to have independent measurements, but now there will be a large smearing effect. It is possible to get to the resolution of a pixel, when pyramidal matching is applied, up to a point where optical flow can to be implemented.

AR: Yes the spacing of the Matching Maps is at the pixel level, and we think this is an advantage of this product rather than a drawback. Indeed, it allows the user to relate directly any pixel of a given orthomosaic to its counterpart in the following orthomosaic, without resorting to an interpolation of the velocity map. This makes the Matching Maps a convenient tool to navigate between the different acquisition dates. In the revised version of the manuscript, this is now clearly stated p 6, l25-27.

Minor comments.

RC: p1 l1 high-frequency -> inter-seasonal; p1 l1 image -> elevation and velocity

AR: For now we decided to not change the title of the paper. Indeed, we think that inter-seasonal can be misleading because almost only summer months are covered, and we prefer to emphasize more on the raw data (i.e. UAV based images) than on the processing (elevation and velocity).

RC: p1 l13 new dataset -> new topographic dataset

AR: Ok.

RC: p1 l13 intensive: subjective text, I am aware this is hard work but not necessary information for the abstract

AR: Ok. We removed this text.

RC: p1 l14 summer 2017 -> summer of 2017
p2 l7 summer 2017 -> summer of 2017

AR: Ok.

RC: p1 l17 displacements and velocity, choose one as these are two words for the samething.
p2 l17 displacements and velocities; choose one

AR: Ok. We chose ‘displacements’.

RC: p2 l8 -> "10 consecutive DEMs and associated orthomosaics"; you first need to make a DEM in order to be able to make a mosaic

AR: This is right. We modified the manuscript accordingly (p 2, l7)

RC: p2 l9 surface evolution.

AR: Ok.

RC: p2 l23 "ice flow dynamics at the surface" I think the emergence velocity by [Brun 2018] is also a good example of a process. Furthermore, mentioning the use of multitemporalDEM’s as in [Wang , Berthier] might be worth it as well.

AR: Thank you for drawing our attention on these references. They are now used to better contextualize our work at the end of the introduction (p 2, l17-25).

RC: l1 "6%" maybe also specify in degrees

AR: Ok.

RC: p3 l4 "mainstream" -> central flowline?

AR: Ok.

RC: p3 l19 maybe include the lake location, which drains, and also include the ELA?

AR: The lake was moraine-dammed and disappeared some years ago due to glacier retreat. Regarding the ELA we think that it is roughly visible in the background orthomosaic in Fig 1b which has been acquired at the end of the summer.

RC: p5 l3 pix4D, please give the version

AR: Ok.

RC: p5 l7 swap orthomosaic and DEMs

AR: Ok.

RC: p5 l9 UTM_zone32 -> Universal Transverse Mercator (UTM zone 32)

AR: Ok. In addition, we better explain the georeferencing of the master bundle adjustment (p 6, l3-4).

RC: p5 l12 I assume all flights are nadir, or did the UAV also took oblique imagery. This isof interest, as it enhance the separation between internal parameters [james 2014].

AR: Yes all flights are close to nadir. In the revised version of the manuscript we specify it p 4, l4-5.

RC: p6 l1 "GCPs" is maybe not the correct term, as they are not real ground control, hence (manual) tie-points might be more correct.

AR: We agree with 'manual tie points'. We adopted this terminology throughout the revised manuscript.

RC: p6 l10 51x51 pixels, also include the metric size, that is roughly 5 meters right?
p6 l12 2000 pixels, see former comment

AR: Ok.

RC: p7 l10 "locations with strong spatial gradients", this is not a very effective post-processing step. It is very local and isolated inliers will also be removed. More advanced post-processing techniques are possible [maksymiuk 2016], but I am not asking to do this, just so you are aware of such studies.

AR: We agree that our post-processing approach is rather simple. We therefore clearly state it in the revised manuscript (p 7, l24-26). In addition we added the reference suggested by Reviewer#1.

RC: p7 l16 "are interpolated", which type/method?

AR: We used a bilinear interpolation. This is now mentioned p 7, l34.

RC: p7 l16 "reliable measurements", not correct wording, there is no real testing, thus reliable is misplaced here.

AR: We reformulated this sentence (p7, l34) and changed 'reliable' to 'non-masked'.

RC: p8 l1 the east and northward components do not seem to be the same....? also, why is the displacement given in pixel and not in a metric scale?

AR: We did not understand the first part of the comment. Maybe a color issue? In any case Fig 3 has been redesigned according to a comment of the Editor. We hope that this change helps.
Regarding the second part of the comment, displacements are given in pixels because the unit of the Matching Maps is pixel. Displacements in m/day are shown on Figure 5.

RC: p8 l14 There seem to be multiple flights per campaign. Because a fixed wing is used, the landing must have had an impact. Hence, internal camera parameters might been different between different flights. Thus, are these groups of data also separated in the camera optimization?

AR: Yes there are multiple flights per campaign, and they are processed all together. This is now clearly stated p 5, l3.
Since the SODA camera we used is specially designed for ebee flights (and associated possible rough landings) it is supposed to be robust to landing conditions. Hence, the camera parameters are expected to not change much between flights.
To verify it, we plotted the camera parameters estimated for each date. In case of changing camera parameters induced by landing, different dates should have rather different estimated parameters. This is fortunately not the case. The estimated camera parameters are pretty stable along time (see figure R1.4 below), except one big 'jump' between July 13th and July 26th. This jump is due to the change of the camera, the device used for the first five acquisition dates having been destroyed in a UAV crash between these two dates during another (independent) project. It does not affect our data because the camera was never changed between the flights used for a single orthomosaic. In conclusion, we believe that the camera parameters are pretty stable along time, and are not much affected by the intra-campaign landings within a single day.

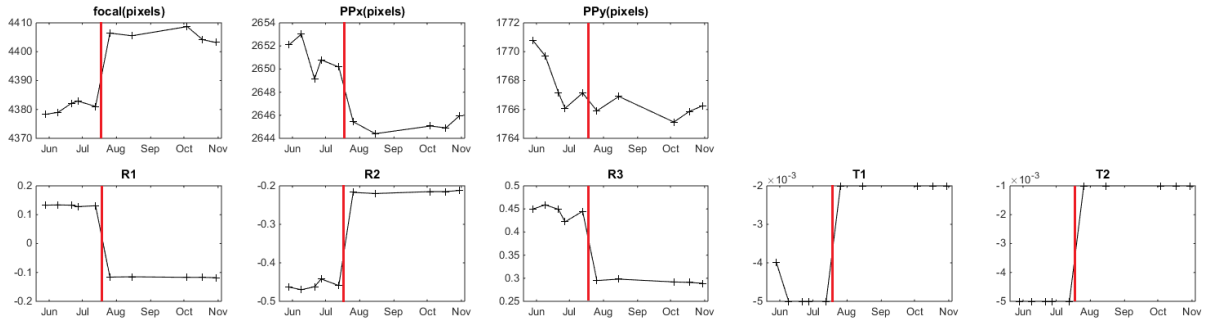

Figure R1.4: temporal variability of estimated internal camera parameters. Vertical red lines denote a change of camera (between 07/13 and 07/26).

RC: p9 l3 are due -> can be

AR: Ok.

RC: p10 l11 "smooth out local variability", why is this done? and why is the mean taken, and not more robust measures like the median?

AR: Just to remove possible imperfections. But the formulation of this sentence was misleading. We removed this part of the sentence.

RC: p11 l12 why are single points used as validation, it might be good to look at stable terrain as well. The Randolph glacier mask can exclude glacial terrain, the rest can be used to create a histogram of displacements.

AR: Points located in stable terrain are also used for validation. We emphasize it in the revised manuscript (p 11, l 4). These are the green dots (and associated velocities) in Fig 5. The apparent displacements of these supposedly static locations are therefore used to estimate the precision of the velocities derived from the Matching Maps, and reported in Fig 5b.

RC: p11 l12 "since the area of interest", is only the icefall of interest? Are other features on the glacier tongue of interest as well (meander evolution of supra glacial streams, emergence velocity ....)?

AR: This is right, the icefall is not the only area of interest. This sentence has been modified to avoid misinterpretation (p 12, l1).

RC: p13 l4 "for almost any glacier mapping task", not specific and does not hold either, please rephrase.

AR: Ok.

Responses to the comments of Reviewer #2:

In the following point-by-point reply, RC denotes a reviewer comment and AR denotes our response to the comment.

RC: In this case it appears the authors used the later method relying on consumer grade GPS positions of the UAV to generate the 9 June orthomosaic and DEM, all other datasets are then coregistered to this 'master' dataset using stable bedrock features. What this means is that the stacks themselves are co-registered accurately and we can therefore observe changes between images pairs fairly precisely. However, the master 9 June dataset is likely to be so inaccurate positionally that any measurements made from these data are likely to be highly inaccurate.

AR: We agree with the fact that based on consumer grade GPS data, the initial geo-referencing of our dataset is not precise. To warn the reader about it, a new paragraph has been added at the end of the section 3.1 (generation of co-registered orthomosaics and DEMs, p 6, l1-13). This paragraph details the impact of the absence of GCPs on the geo-referencing of the master bundle adjustment, and mentions that internal deformations can also occur. To better geo-reference our dataset, we followed the option (3) proposed by reviewer#2. We therefore co-registered the master orthomosaic on an orthomosaic processed by the Swiss Mapping Agency. The parameters of the transformation allowing to link our dataset to the Swiss reference system are given in Table 2 of the revised manuscript.
Regarding the internal deformations, they are now assessed by studying the residuals of aforementioned co-registration procedure. The amplitude of these deformations is discussed in details at the end of the section 4.1 dedicated to the quality assessment of the orthomosaics (p 9, l15-22 -> p10, l 1-7). In addition, the residuals of the co-registration procedure are displayed in the revised Fig 4 and are relatively small. Furthermore, we show that the influence of these deformations has a very small impact on the estimated velocities (see our replies to the next comment).

RC: Below I have outlined a few potential methods for remedying this issue. 1) Install ground control targets in the survey area and conduct another survey of the glacier, then use this as the master dataset to co-register the other datasets to, using stable/no change locations. This is that was done in the (Immerzeel et al., 2014; Kraaijenbrink et al., 2016) articles that the authors use as justification for the co-registration method they employed. Obviously installing ground control targets on glaciers and over a large area is extremely difficult and often not possible given access, safety and logisitical challenges. This is one of the major limitations of collecting research grade UAV datasets over challenging environments. Because of these limitations we are often forced to live with poorly distributed or inadequate numbers of ground targets. In the glacier context this means ground control is often restricted to installations along the moraine edges, but even this is much better than none. And, would in my opinion provide an acceptable product in line with other UAV/glacier publications. Furthermore, the authors did use some 'on-ice' GNSS data to assess the accuracy of the velocity measurements - these stations could be used in conjunction with moraine ground control targets alongside perhaps two more on ice targets - e.g. one near terminus, one near middle, limiting labour/time investment. 2) Fly a UAV equipped with L1 or L1/L2 differential GNSS and use an RTK or PPK positional solution to derive a more accurate master data set. Then use this dataset to co-register the other dates. An example of this method as applied to glaciers is currently under review in the cryosphere discussions: Chudley et al., 2018. 3) If there is a high quality DEM and imagery data from other sources e.g. LiDAR/airborne imagery/high resolution satellite data, then authors could extract ground control positions from these data and co-register the UAV datasets to this.

AR: As mentioned above, we adopted the solution (3) proposed by Reviewer#2 to better geo-reference our dataset and to assess the amplitude of the internal deformations. The revised Fig 4 shows that the internal deformations have a metric amplitude and are smoothly spread over the target area. Taking into account the size of the area of interest, the relative errors induced by the internal deformations are therefore of the order of 1/1000. When propagating in Matching Maps, these internal deformations lead to errors <1mm/day on the estimated surface velocity, which is very small in regard to the amplitude of the ice surface velocity signal (around 30cm/day). To warn the reader about the potential impact of the internal deformations on our dataset, a comprehensive uncertainty analysis is now reported in a new paragraph added at the end of section 4.1 (p9, l15 -> p10, l6).

RC: Finally, I have read the other posted review for this paper and agree with their suggestions regarding the matching maps. Further description of how these were derived is needed as they are non-standard, and ideally more widely used methods for velocity field derivation should be applied – e.g. COSI-CORR as this would be 1) easier to follow, 2) likely to be more useful to other researchers.

AR: As mentioned in our response to the comments of Reviewer#1, we completely revised the section dedicated to the generation of Matching Maps (in particular p 6, l 20 -> p 7, l 20) in order to better describe this product.
In addition, to ensure that our Matching Map Maker utility is reliable, we benchmarked against velocity maps calculated using the well-established CIAS and Imcorr algorithms. The results show that our method does not introduce any bias or inconsistencies. To reassure the user about the reliability of our utility, we added the results of the benchmarking tests in a sub-directory of the repository of the Matching Map Maker utility. In addition, we mention the existence of these tests (and the associated results) in the manuscript (p7, l16-18 and p13, l7-13).

RC: Additional points: To prevent the use of incorrect data by others the authors should clip out obviously erroneous regions in the DEM and orthomosaic, i.e. along the edges of the survey area.

Ideally all datasets could be clipped to a common extent boundary and raster grid for ease of use, though this is less important.

AR: We prefer to warn the user about the limitations of the dataset rather than clipping the 'best' areas. To this end, we provide in the dataset a processing report for each pair DEM + orthomosaic. These reports allow the user to identify, for each acquisition date, in which areas our products fulfills its needs for a given application. Regarding the Matching Maps, unreliable areas are masked, as highlighted in the revised version of Fig 3. The reliability masks are available along with the Matching Maps.

Responses to the comments of the Editor:

In the following point-by-point reply, EC denotes an editor comment and AR denotes our response to the comment.

EC: I understand that you have used a commercial software package for the bulk part of the processing. This is ok, however, I believe the underlying algorithms should be explained/mentioned explicitly so that your study remains reproducible. For example, for people without access to pix4D Mapper, it is not helpful to state that the "default values" (p5/l5) were chosen.

AR: We modified the first paragraph of section 3.1 to better explain the photogrammetric processing using Pix4D (p 5, l3-10).

EC: Fig. 5 has peculiar gray box behind that image which should be removed (maybed this is PDF viewer dependent? I have used Preview on MacOS.

AR: We modified figure 5 to make it more clear. To this end, the ice surface velocity is now displayed with contour lines rather than a background color. We hope that this change also improves the visual aspect of the figure.

EC: Consider changing the chosen colormaps to a sequential colormap. The rainbow colormaps (and their relatives) are prone to introduce false boundaries (e.g. https://www.climate-lab-book.ac.uk/2016/why-rainbow-colour-scales-can-be-misleading/ by Ed Hawkins).

AR: Fig 3 has been edited, and in the new version a grayscale colormap is used.

EC: Fig. 1c: Label Zwilings-GL is hard to read. Maybe move it to the heaven-part of the picture and use arrows? Not sure.

AR: Ok.

A high-frequency and high-resolution image time series of the Gornergletscher - Swiss Alps - derived from repeated UAV surveys

Lionel Benoit[1], Aurelie Gourdon[1,2], Raphaël Vallat[1], Inigo Irarrazaval[1], Mathieu Gravey[1], Benjamin Lehmann[1], Günther Prasicek[1,3], Dominik Gräff[4], Frederic Herman[1], Gregoire Mariethoz[1].

[1]Institute of Earth Surface Dynamics (IDYST), University of Lausanne, Lausanne, Switzerland.
[2]Ecole Normale Supérieure de Lyon, Département des Sciences de la Terre, Lyon, France.
[3]Department of Geography and Geology, University of Salzburg, Salzburg, Austria.
[4]Laboratory of Hydraulics, Hydrology and Glaciology (VAW), ETH Zürich, Zürich, Switzerland.

Correspondence to: Lionel Benoit (lionel.benoit@unil.ch)

Abstract. Modern drone technology provides an efficient means to monitor the response of alpine glaciers to climate warming. Here we present a new topographic dataset based on images collected during ten UAV surveys of the Gornergletscher glacial system (Switzerland) carried out approximately every two weeks throughout the summer of 2017. The final products, available at: https://doi.org/10.5281/zenodo.1487862 (Benoit et al, 2018), consist of a series of 10 cm resolution ortho-images, digital elevation models of the glacier surface, and Matching Maps that can be used to quantify ice surface displacements. Used on its own, this dataset allows mapping the glacier and monitoring surface velocities over the summer at a very high spatial resolution. Coupled with a classification or feature detection algorithm, it enables extracting structures such as surface drainage networks, debris or snow cover. The approach we present can be used in the future to gain insights into ice flow dynamics.

1 Introduction

Glacier ice flows by deformation and sliding in response to gravitational forces. As a glacier moves, internal pressure gradients and stresses create visible surface features such as glacial ogives and crevasses (Cuffey and Paterson, 2010). Furthermore, the surface of glaciers is also shaped by local weather conditions, which are responsible for the snow accumulation and ablation. Related processes generate distinct morphologies such as supra-glacial streams, ponds and lakes.

Glacier surface features evolve continuously, and these changes provide insights into the structure, internal dynamics and mass balance of the glacier. Important efforts have been made to monitor glacier surfaces, from early stakes measurements at the end of the 19th century (Chen and Funk, 1990) to present-day in-situ topographic surveys (Ramirez et al, 2001; Aizen et al, 2006; Dunse et al, 2012; Benoit et al, 2015) and remotely sensed data acquired from diverse platforms: ground-based devices (Gabbud et al, 2015; Piermattei at al, 2015), aircrafts (Baltsavias et al, 2001; Mertes et al, 2017) or satellites (Herman et al, 2011; Kääb et al, 2012; Dehecq et al, 2015; Berthier et al, 2016a). Recently, the development of Unmanned Aerial Vehicles (UAVs) has enabled glaciologists to carry out their own aerial surveys autonomously, rapidly, and at reasonable costs

(Whitehead et al, 2013; Immerzeel et al, 2014; Bhardwaj et al, 2016; Jouvet et al, 2017; Rossini et al, 2018). This technology is particularly attractive to map alpine glaciers whose limited size allows a satisfying coverage at a centimeter to decimeter spatial resolution.

Here we provide a homogenized and high-resolution remote sensing dataset covering about 10 km^2 of the ablation zone of the Gornergletscher glacial system (Valais, Switzerland, Fig 1). The raw images have been acquired by UAV flights carried out approximately every two weeks during the summer of 2017 (from May 29 to October 30). The dataset comprises 10 consecutive Digital Elevation Models (DEMs) and associated ortho-mosaics of the area of interest at a 10 cm resolution. It is therefore one of the most exhaustive surveys of the short-term surface evolution of a temperate glacier currently available. Geometrical coherence of the dataset is ensured through the application of a comprehensive photogrammetric processing (i.e. images are ortho-rectified and properly scaled). In addition, the orthomosaics are stackable thanks to a co-registration procedure. The dataset can therefore be seen as a high resolution time-lapse of the Gornergletscher ablation zone, combining spectral (orthomosaics) and geometrical (DEMs) information on the glacier surface. In addition to orthomosaics and DEMs that are snapshots of the area of interest, we also provide a product that we call Matching Maps (MMs) to achieve a temporal monitoring of the glacier. In practice, a Matching Map associates to each pixel of an orthomosaic (respectively a DEM) the corresponding pixel in the next orthomosaic recorded two weeks later. MMs can then be used to track the flow of ice over time, and in turn to quantify ice surface displacements.

Potential uses of this dataset are numerous. Single orthomosaics and DEMs can be used to map the surface of the glacier and to extract features of interest such as the surface drainage network (Yang and Smith, 2012; Rippin et al, 2015), debris or snow cover (Racoviteanu and Williams, 2012). Alternatively, the complete time series of orthomosaics and DEMs can be used for detection and quantification of changes at the surface of the glacier (Barrand et al, 2009; Berthier et al, 2016b; Fugazza et al, 2018). Finally, the time-lapse coupled with the Matching Maps is an interesting tool to monitor ice surface velocity and deformation (Ryan et al, 2015; Kraaijenbrink et al, 2016), and in turn ice flow dynamics at the glacier surface (Brun et al, 2018). The Matching Maps provide a quantification of the ice velocity at every location on the surface of the glacier, which can be used to calibrate or to validate ice flow models, especially for the Gornergletscher which was extensively used as a modeling benchmark (see for instance Werder and Funk, 2009; Riesen et al, 2010; Sugiyama et al, 2010; Werder et al, 2013).

2 Data acquisition

2.1 Study site

The Gornergletscher is located in the Valais Alps in southern Switzerland (Fig 1a). It is part of a glacier system involving five tributaries and ranges from 2200 m to 4634 m a.s.l. (Fig 1b). The ablation area, which is the main focus of this study, is a 4km long and relatively flat ice tongue (slope around 6 % i.e. 3.4°) that is deeply incised by meltwater channels and partially debris

covered (Fig 1c). This ablation area is preceded by a steeper part (south-west of the Monte Rosa Hütte, Fig 1c) characterized by the presence of numerous crevasses. The entire Gornergletscher system (i.e. the terminal tongue and its five tributaries) covers an area of almost 50 km^2 and its central flowline is 12 km long, making it one of the largest European glaciers (Sugiyama et al, 2010).

The Gornergletscher system has been widely studied since the 1970s due to its significant size, its accessibility, and because a glacier-dammed lake threatened the downstream Matter valley with glacier outburst floods (Sugiyama et al, 2010; Werder et al, 2009; Werder et al, 2013). The long history of glaciological studies in this area has shown that the mass balance of the Gornergletscher system was stable from the 1930s to the early 1980s, and significantly dropped since then (Huss et al, 2012). This can be associated with the rise of its Equilibrium Line Altitude (ELA) due to an increase of the local average yearly temperature. The ELA stands nowadays around 3300m according to studies carried out at the neighboring Findelgletscher (Sold et al, 2016).

In this context, the current dataset aims at complementing existing studies about the Gornergletscher system by documenting the behavior of its ablation zone during an entire summer, at a time when this glacial system is thought to be out of equilibrium with a clear trend toward glacial retreat. In particular, this dataset focuses on the monitoring of the glacier surface at high spatial and temporal resolution.

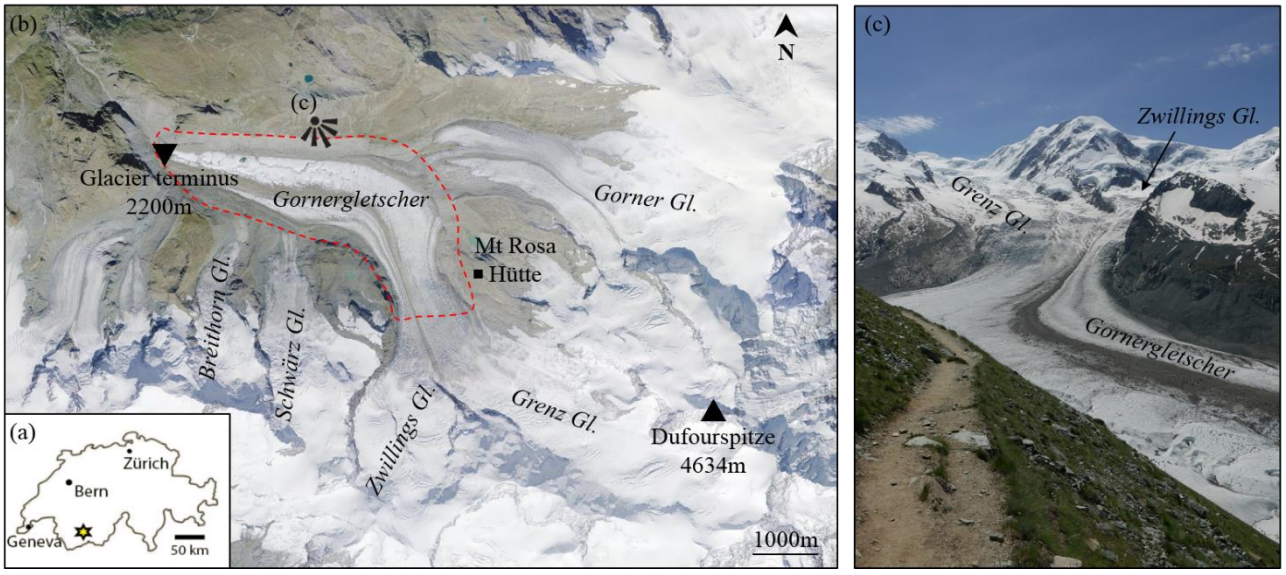

Figure 1: The Gornergletscher system. (a) Situation map; (b) overview of the Gornergletscher system, dashed red line: area of interest; (c) picture of the glacier tongue.

2.2 UAV surveys

The primary data are RGB images acquired by repeated UAV surveys over an area of 10 km^2. A fully autonomous fixed-wing UAV of type eBee from SenseFly, equipped with a 20 megapixels SenseFly S.O.D.A camera, has been used for image acquisition (Vallet et al, 2011). The camera was static within the UAV body (no Gimbal) and therefore all pictures are quasi-nadir (i.e. images are taken with an angle +/- 10° from the vertical line). For flight planning and UAV piloting, the eMotion3 software was used.

Raw images were acquired with a ground resolution ranging from 7.3 cm to 8.8 cm for the glaciated parts of the area of interest. For the requirements of photogrammetric processing, flight plans have been designed to allow for an overlap between images ranging from 70% to 85% in the flight direction, and from 60% to 70% in the cross-flight direction. These specifications have led to flight altitudes ranging from 300 m to 600 m above ground. The flight time was limited to about 30 min in field conditions. Thus, the coverage of the full area of interest required 4 to 8 separate flights per session, i.e. each day of acquisition (Table 1). Overall, 10 sessions have been conducted in 2017, from May 29 to October 30. The main features of these flights are summarized in Table 1:

Date	Acquisition Time (CET)	# of flights	# of pictures
2017/05/29	14:00 – 16:00	4	749
2017/06/09	12:30 – 15:30	8	935
2017/06/21	11:30 – 13:30	7	930
2017/06/27	11:30 – 14:00	5	1059
2017/07/13	12:30 – 14:00	4	830
2017/07/26	13:00 – 16:00	6	1125
2017/08/15	12:30 – 16:00	7	1121
2017/10/04	12:00 – 15:30	7	1107
2017/10/18	13:00 – 15:00	4	846
2017/10/30	13:00 – 15:30	6	1084

Table 1: UAV flights carried out for raw glacier image acquisition.

3 Data processing

3.1 Generation of co-registered orthomosaics and DEMs

Pictures have been processed separately for each acquisition date with the photogrammetric software pix4DMapper version 3.1 ((Vallet et al, 2011), Fig 2) using default parameters for nadir flights (see the processing reports for details about these parameters). The output resolution has been set to 10 cm/pixel in order to prescribe a constant resolution across all final products. During the photogrammetric processing, the raw pictures are first oriented by bundle adjustment, and then a DEM and an ortho-rectified image (orthomosaic) are generated for each day of interest. Since the only geolocation information included into the bundle adjustment procedure is the trajectory of the UAV derived from code-only GPS data, the initial geo-referencing of the orthomosaics and DEMs is limited to a few meters.

To improve the coherence of the co-referencing of the different sessions, all products are co-registered to the reference of the June 9 acquisition (Fig 2). To this end, the coordinates of several stable points of the landscape (16 to 70 among a set of 74, see Table 2 and Fig 4) are extracted from the bundle adjustment of June 9, and used as manual tie points for the bundle adjustments of the other dates. These stable points are mostly salient features of the bedrock or erratic boulders on the deglaciated banks of the glacier. The co-registration leads to orthomosaics and DEMs that are stackable. Therefore, in the final products, the bedrock remains stable between consecutive dates, while the glaciated parts move and deform. Consequently, if a time-lapse is created from the co-registered products, the glacier appears to flow while the surrounding landscape remains static. Fig. 2 summarizes the acquisition and processing chain used to derive the final products of the dataset.

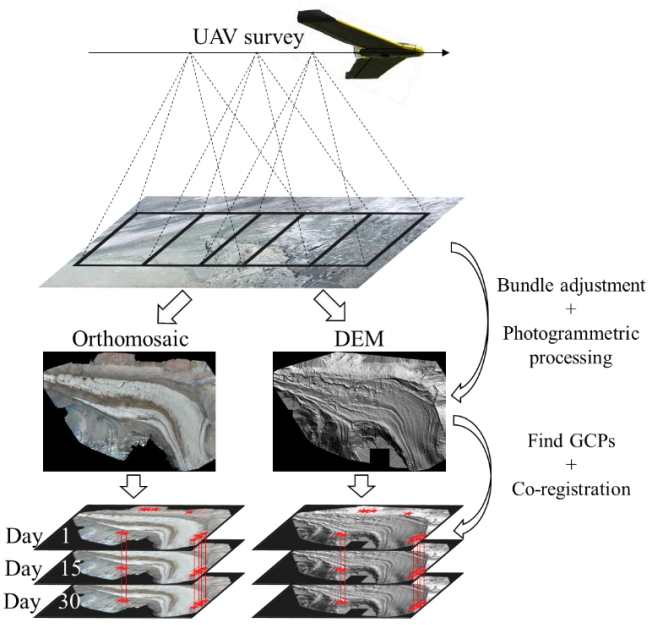

Figure 2: Acquisition and processing chain used to derive the co-registered orthomosaics and DEMs

After co-registration, all final products (orthomosaics and DEMs) are in the reference frame of the bundle adjustment of June 9 2017 (hereafter referred to as master bundle adjustment). This local reference frame is a realization of the WGS84 reference system (with Universal Transverse Mercator (UTM zone 32) projection) using code-only GPS data as input for referencing. The absence of Ground Control Points (GCPs) and the use of consumer-grade GPS observations in the bundle adjustment procedure can result in meter-level geolocation errors and internal deformations of the master bundle adjustment (James and Robson, 2014; Gindraux et al., 2017). While the internal deformations of the local reference frame lead to relative measurement errors of small amplitude (on the order of 1/1000, see Sect. 4.1 for details), the geolocation errors related to the absence of GCPs can impair comparisons with other datasets covering the same geographic area. To improve absolute georeferencing and to link our dataset with the Swiss national reference system, Table 2 provides the parameters of the affine transformation between the local reference frame of this dataset and the Swiss CH1903 – LV 03 reference system. This transformation has been estimated from 81 manual tie points identified in (1) the orthomosaic derived from the master bundle adjustment and (2) a 50 cm resolution orthomosaic of 2009 processed and georeferenced by the Swiss mapping agency SwissTopo.

Translation Eastward (m)	Translation Northward (m)	Rotation (°)	Scale
321800.8	-5009609.3	1.1357	1.0004

Table 2: Parameters of the affine transformation between the Swiss reference system (CH1903 – LV03) and the local reference frame defined by the master bundle adjustment of 2017 June 9. Note that no shear nor reflection is considered. Locations of the manual tie points used to estimate the transformation parameters are shown in Fig. 4.

3.2 Surface displacement tracking: generation of Matching Maps

Consecutive co-registered orthomosaics enable to quantify horizontal displacements at the surface of the glacier. In the present dataset, this information about ice surface displacements is provided by the Matching Maps (MMs, Fig 3). In practice, a MM is an image that pairs the positions of similar ice patches at times t and $t+dt$ (dt being the time span between consecutive acquisitions) (Fig 2). The footprint of the MM is the overlap of the footprints of the orthomosaics at times t and $t+dt$. It follows that a MM is a map of the horizontal displacements occurring at the surface of the Gornergletscher between two consecutive UAV acquisitions. MMs inherit the spatial resolution of the original orthomosaics (i.e. 10 cm) and can therefore be used either to relate directly any pixel of a given orthomosaic to its counterpart in the following orthomosaic (and therefore easily navigate within the whole dataset), or to estimate surface flow velocities.

The MMs are obtained by image matching of pairs of orthomosaics. The orthomosaic at time t is taken as a reference, and for each pixel of the reference, a 51 x 51 pixels (5.1 m x 5.1 m) patch is extracted and searched for in the orthomosaic corresponding to the next session (time $t+dt$). To speed up the processing and avoid wrong matches with very distant patches,

the homolog patch at time $t+dt$ is searched for in a neighborhood with a 200 pixels (20m) radius centered on the position of the original patch at time t whose size has been established based on prior knowledge about the approximate surface velocity of the Gornergletscher. The criterion used to evaluate the similarity between both patches is the mean absolute error (MAE) between pixels computed on grayscale images (Liu and Zaccarin, 1993; Chuang et al, 2015). The MAE has been selected as similarity score because it is fast to compute, especially on large images using convolutions. Its disadvantage is the sensitivity to illumination differences between consecutive orthoimages. However, in practice, no adverse effects have been observed, mostly because the images were acquired roughly at the same time of the day (between 11:30 and 16:00), and because the orthoimages used to generate the matching maps are always separated by less than one month, which mitigates the illumination differences. The patch of the image $t+dt$ leading to the lowest MAE with the original patch at time t is then considered the counterpart of the original patch. Finally, the displacements (in pixels) between the two patches along the East-West and the North-South directions are recorded into the MM. This operation is repeated for all possible patches in the reference orthomosaic. The MMs have been calculated using an open source utility called MatchingMapMaker developed as part of this project, and made available along with the dataset (See Sect. 5.2 for code availability). The MatchingMapMaker tool has been designed to account for the specificities of UAV-based orthoimages, and in particular their very high resolution. To ensure the reliability of this utility, MMs have been benchmarked against horizontal displacement maps calculated using well-established image correlation algorithms, namely Imcorr (Scherler et al., 2008) and CIAS (Heid and Kääb, 2012). The results of this benchmark (see Sect 5.2) show a very good agreement between horizontal displacement maps derived from MatchingMapMaker, Imcorr and CIAS.

The raw MMs can be noisy due to the presence of outliers in the pattern matching procedure (speckled areas in the raw displacement maps in Fig 3). These outliers originate from the dissimilarity between subsequent orthomosaics, due to, for example, changing shadows or changes at the glacier surface (snowfall, snow or ice melting, etc.). To mitigate the impact of these outliers, we first locate them, then we mask the impacted areas (pink areas in Fig. 3), and finally we interpolate the remaining reliable displacements to fill the gaps generated by the mask. To limit the processing time, a simplistic outlier detection method based on signal processing has been preferred over more sophisticated approaches based on glacier physics (Maksymiuk et al, 2016). Unreliable areas in the raw MMs are assumed to be aggregates of pixels with spatially incoherent displacement values embedded in a matrix of displacements that vary smoothly in space (i.e. the reliable displacements). The borders of unreliable areas are detected as locations with strong spatial displacement gradients, with a detection threshold set to 15 cm of horizontal deformation per day. A mask of reliability is then created by setting the areas with strong gradient to 0 and the remaining of the mask image to 1. The outlier areas (i.e. small aggregates of unreliable values) are then filtered out by applying the opening operator of mathematical morphology to this mask with a structuring element of size 50 x 50 pixels. This operation leads to switch the value of the mask from 1 to 0 for all aggregates of pixels smaller than 50 x 50 pixels. Hence, we obtain a mask with 1 at locations with reliable displacements and 0 where the measured displacements are considered as outliers. Finally, the values of the MM at masked locations are interpolated from the non-masked measurements using a bilinear

interpolation. The selected procedure is iterative. At each iteration, it attributes to the masked values the mean of the reliable values in a 500 pixel neighborhood in the East-West and North-South directions. The values that remain masked after 10 iterations are considered as too far from the informed areas to be filled and are set to -99 to denote no data. Fig. 3 summarizes how MMs are derived from pairs of consecutive co-registered orthomosaics and filtered to remove outliers.

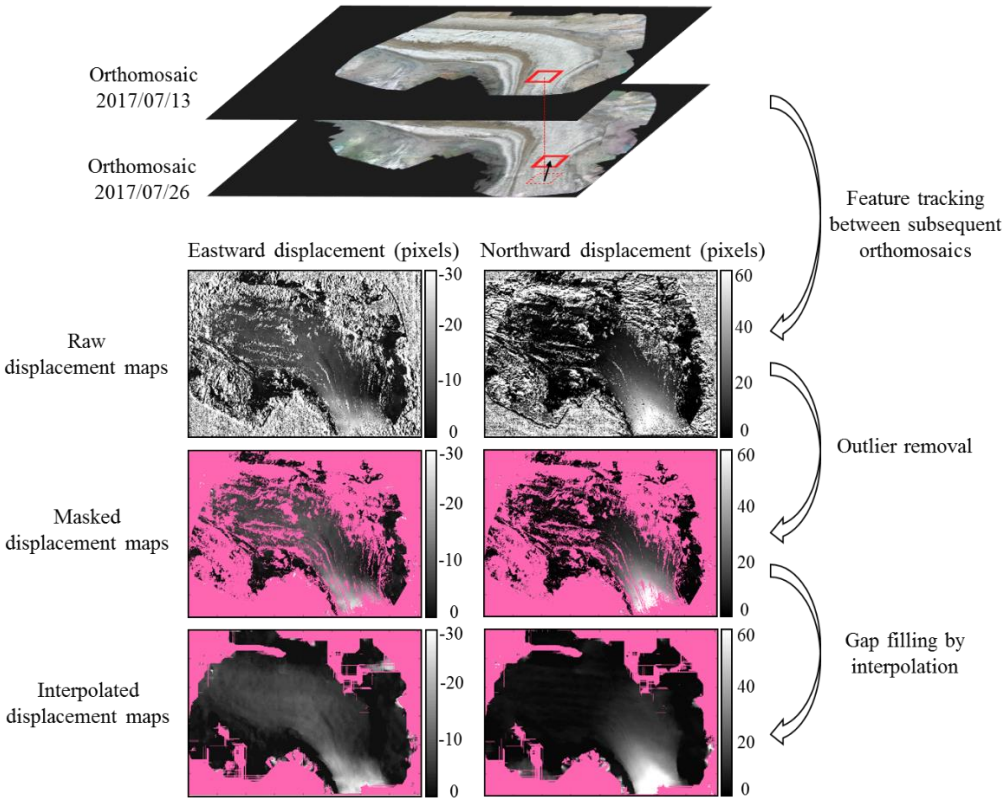

Figure 3: Processing chain used to compute a matching map between two subsequent orthomosaics. The procedure is illustrated for the 2017/07/13 – 2017/07/26 period. In displacement maps, masked areas are displayed in pink.

4 Quality assessment

4.1 Bundle adjustment and co-registration

A first validation of this dataset can be done by checking the relative orientation of the cameras during the bundle adjustment, as well as the co-registration of orthomosaics and DEMs. Processing reports detailing the quality of the bundle adjustment for each session are available along with the dataset (see Sect. 5.1).

Table 2 displays three indices summarizing the quality of both bundle adjustment steps. First, the mean reprojection error (in pixels) quantifies the mismatch in the raw images between the observed and the modelled position of tie points used during

the relative orientation step. The sub-pixel level of errors (Table 2, column 2) ensures that the orientations of the camera are reliable. Next, the co-registration step is assessed by the mean Root-Mean-Square (RMS) error of manual tie point coordinates. This statistic measures the stability of manual tie point coordinates between different bundle adjustments. Under ideal conditions, the value of the mean RMS error on manual tie points should be close to the ground pixel resolution of the raw images (i.e. 7.3 cm to 8.8 cm) because an operator is able to identify points of interest with a pixel level precision. The slightly higher values obtained in the present case (9 cm to 21 cm, Table 2, column 3) can be due to the difficulty of precisely identifying manual tie points under changing environmental conditions (e.g. sunlight exposition or snow cover). The errors in manual tie point identification degrade the mean RMS error, but they are expected to have a mild impact on the co-registration itself because they are not correlated and tend to compensate each other. Note that late in the season (i.e. for the last acquisition on October 30th) it became difficult to identify manual tie points due to strong shadows, hence the small number of manual tie points at that time.

date	Relative orientation: mean reprojection error (pix)	Co-registration: Mean RMS error (m)	Co-registration: # manual tie points
2017/05/29	0.138	0.210	66
2017/06/09	0.136	Reference	Reference
2017/06/21	0.123	0.189	66
2017/06/27	0.146	0.193	68
2017/07/13	0.120	0.107	63
2017/07/26	0.117	0.206	70
2017/08/15	0.118	0.175	69
2017/10/04	0.125	0.122	38
2017/10/18	0.127	0.146	43
2017/10/30	0.125	0.092	16

Table 2: Quality assessment of the bundle adjustment procedure.

Another important validation consists of assessing possible internal deformations within the local reference frame of the dataset. Fig. 4a displays the residuals of the co-registration of the master bundle adjustment on a georeferenced orthoimage, which are a proxy for the internal deformations of the master bundle adjustment. The results show that the internal deformations have a meter-level amplitude (mean deformation = 1.07 m, max deformation = 2.83m) and are smoothly spread over the area of interest due to the bundle adjustment procedure, which tends to distribute errors over space. It follows that, considering the extent of the study area (few square kilometers), the relative error induced by the internal deformations of the local reference frame is on the order of 1/1000. Thanks to the co-registration procedure, the internal deformations of all orthomosaics and DEMs are similar to the ones of the local reference frame defined by the master adjustment. When measuring changes at the

surface of the glacier from the present dataset, the error related to internal deformations is therefore on the order of one per mille of the measured distances. This results in relatively small absolute errors because the changes at the ice surface of the Gornergletscher are of moderate amplitude (e.g. ice ablation reaches few cm/day, and ice flows at less than 1m/day in the ablation zone). For instance, in case of horizontal velocity measurements, the order of magnitude of glacier displacement between two acquisition dates is 30 cm/day x 14 days = 4.2 m. It follows that the error in velocity due to internal deformations is 4.2 m x 1/1000 /14 days=0.3 mm/day, which is very small in comparison with the amplitude of the ice surface velocity itself.

4.2 Orthomosaics and DEMs

In addition to the bundle adjustment, we also validate the final products of the photogrammetric processing (Fig 4a), i.e. the co-registered orthomosaics and DEMs. To this end, individual orthomosaics and DEMs have first been visually checked to track the presence of artifacts. A careful examination of all products shows that the glaciated parts (Fig 4b) as well as the neighboring ice-free areas (Fig 4c) are well reconstructed in both orthomosaics and DEMs. On the edges of the area of interest artifacts can be present due to the low number of overlapping images in these areas (see the processing reports to identify them). This leads to unreliable photogrammetric reconstructions and in particular shear lines (Fig 4d). Despite these relatively minor artifacts restricted to the edges of the surveyed area, all glaciated parts and nearby unglaciated margins are satisfyingly reconstructed in both orthomosaics and DEMs.

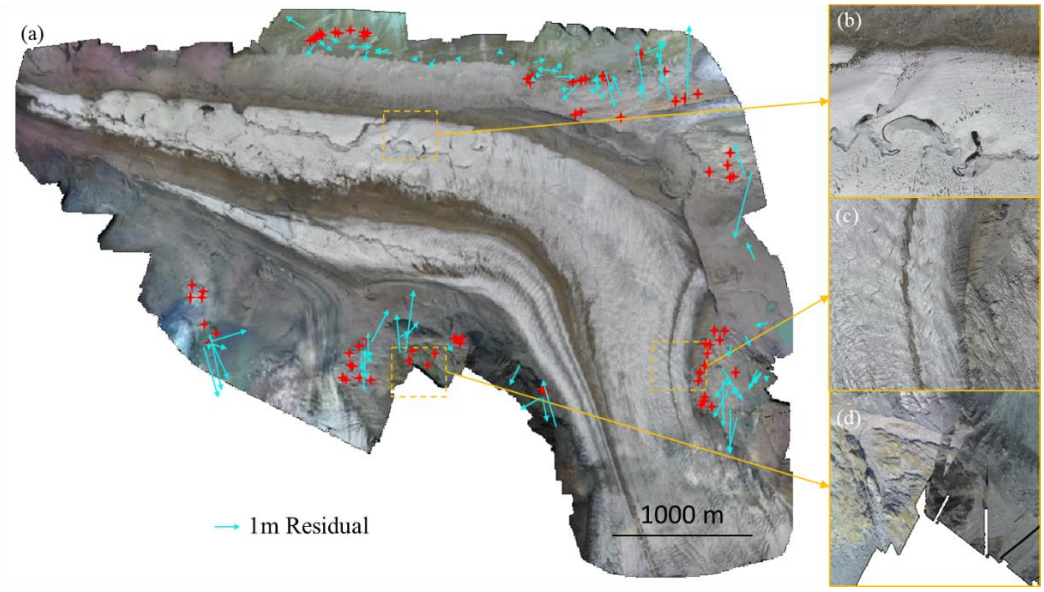

Figure 4: Quality assessment of the orthomosaics. (a) Overview of one orthomosaic (2017/08/15). Red stars: manual tie points used for co-registration. Blue arrows: residuals after co-registration of the master bundle adjustment on a 50 cm-resolution orthoimage acquired in 2009. The affine transformation described in Table 2 has been used for co-registration. (b) - (c): Examples of areas where the photogrammetric processing worked properly. (d): Example of area on the boundary of the domain where the photogrammetric processing produced artifacts (mostly shear lines).

4.3 Matching Maps

In addition to the visual inspection of individual photogrammetric products, we also assess the quality of the co-registration procedure by quantifying in the MMs the stability of several areas that are most likely static, as well as the observed spatial patterns of glacier surface velocity. We select several validation locations on and off the glacier (Fig 5) and compute their horizontal velocity by dividing the displacements recorded in the MMs by the time elapsed between the acquisitions. Note that in Fig. 5 the velocity is averaged over 10 x 10 m^2 areas, corresponding to 10000 single measurement points, centered on the validation points.

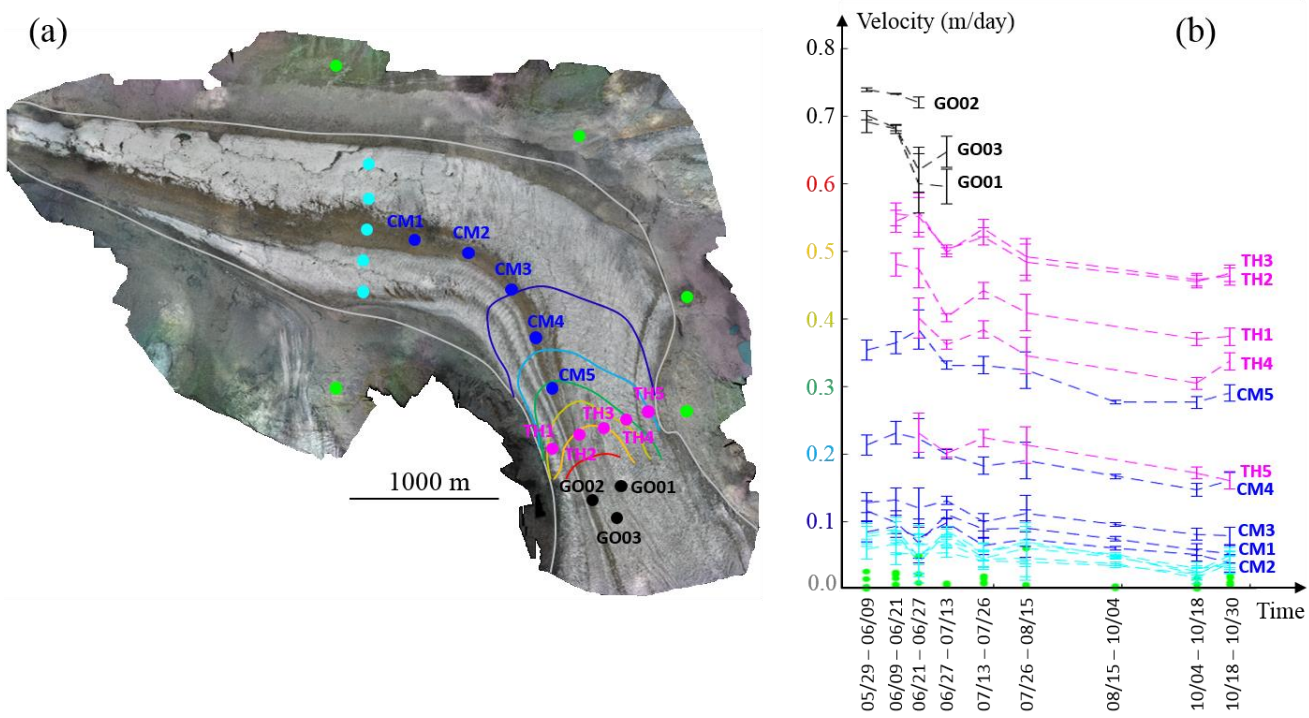

Figure 5: Quality assessment of the Matching Maps. (a) Locations of the validation points. The contour lines represent the horizontal surface velocity derived from the MM related to the period 07/13 – 07/26. (b) Observed horizontal surface velocities at validation locations. Error bars show 1σ errors. The errors reported for UAV-based velocities are empirical errors and are equal to the quadratic mean of velocities recorded at ice-free locations (green dots in (b)). The errors reported for GNSS-based velocities (i.e. at locations GO01, GO02 and GO03) are theoretical errors accounting for the uncertainty induced by the tilt of the support of GNSS receivers over time due to glacier movement.

Fig. 5b displays the observed horizontal velocities in the domain for summer 2017. In case of perfect photogrammetric processing, co-registration, and feature tracking, the apparent velocity of the ice-free areas (in green on Fig 5) should be zero. While it is not exactly the case due to inherent processing errors and measurement noise, the mean velocity is very low (1.2

cm/day on average over the 5 ice-free validation locations) which reflects an appropriate processing. The observed patterns of glacier surface velocity are also in accordance with typical patterns of ice flow, such as velocities decreasing from the center of the glacier towards the edges (compare e.g. the velocity in TH3 and TH5) and higher velocities at steep parts of Grenzgletscher than on the flat tongue of Gornergletscher (compare e.g. TH2 and CM5 to CM1). Finally, the velocities derived from UAV correspond to independent data collected by differential GNSS measurements a few hundred meters upstream of the area of interest (points GO01, GO02 and GO03 in Fig 5). The higher velocity measured at the locations monitored by GNSS (points GO01-G003) compared to the downstream locations monitored by UAV (points TH1-Th3) is coherent with the increase of glacier velocity at the steeper upstream part of Grenzgletscher (approx. 13.5 % at GO02 compared to 7.5 % at TH2). Finally, the trend of deceleration over the course of the summer recorded by GNSS is in good agreement with the UAV-based velocities throughout the glacier.

5 Data and code availability

5.1 Structure and availability of the dataset

All the data presented in this dataset are available in the following repository (Rep): https://zenodo.org/record/1487862, with the following DOI: https://doi.org/10.5281/zenodo.1487862 (Benoit et al, 2018).

The results of the photogrammetric processing, i.e. the orthomosaics and the DEMs, are available in the compressed folder Rep\Photogrammetric_Products.zip. Within this folder, the products are grouped in sub-folders by acquisition date using the following standard: 2017_mm_dd with 'mm' the month and 'dd' the day of acquisition. Finally, these sub-folders contain the following files:

- 2017_mm_dd_orthomosaic.tiff: Contains the orthomosaic.
- 2017_mm_dd_dem.tiff: Contains the DEM.
- 2017_mm_dd_report.pdf: Contains the processing report (generated by Pix4D Mapper) that summarizes the quality of the photogrammetric processing for the date of interest.

The Matching Maps are stored in the compressed folder Rep\Matching_Maps.zip. Within this folder, the individual maps are grouped in sub-folders named according to the acquisition date of the pair of subsequent orthomosaics used to generate the Matching Map: 2017_mm_dd_2017_nn_ee with 'mm' (resp. 'dd') and 'nn' (resp. 'ee') the acquisition months (resp. days). These sub-folders contain the following files:

- 2017_mm_dd_2017_nn_ee_disp_Eastward: Contains the Matching Map of Eastward displacements.
- 2017_mm_dd_2017_nn_ee_disp_Northward: Contains the Matching Map of Northward displacements.

- 2017_mm_dd_2017_nn_ee__disp_mask: Contains the mask of reliable displacements after filtering: 1 if the location corresponds to a reliable displacement, 0 otherwise.

5.2 Code availability

The photogrammetric processing has been carried out using the proprietary software Pix4D Mapper, commercially available at: https://pix4d.com/ (last access 2018/11/16).

The Matching Maps have been computed using Matlab routines written by Mathieu Gravey. The related utilities are freely available on the following repository: https://github.com/GAIA-UNIL/MatchingMapMaker. The sub-repository Benchmarking_tests contains the results of benchmarking tests aiming at comparing the displacement maps computed by the MatchingMapMaker utility (i.e. MMs) with displacement maps computed by well-established glacier surface tracking algorithms, namely Imcorr (https://nsidc.org/data/velmap/imcorr.html) and CIAS (https://www.mn.uio.no/geo/english/research/projects/icemass/cias/). The sub-repository Similarity_score_tests contains the results of tests assessing the sensitivity of the MatchingMapMaker output to the similarity score used to define patch matches.

6 Conclusion

The present dataset compiles ten UAV surveys of the Gornergletscher carried out during summer 2017. Photogrammetric processing leads to a set of 10 cm resolution orthomosaics, DEMs and glacier displacement maps for each acquisition date. This dataset can be used for change detection and quantification at the glacier surface, and in particular to investigate glacier surface dynamics at high temporal and spatial resolution.

Author contributions

AG, FH and GM designed the experiment.
AG, RV, II, BL, GP and LB carried out the acquisitions.
AG, RV and LB performed the photogrammetric processing.
MG, LB and AG computed the Matching maps.
DG recorded differential GNSS data used for validation.
LB wrote the manuscript with inputs from all authors.

Competing interests

The authors declare no competing interests.

Acknowledgments

The authors are grateful to Philippe Limpach from ETH Zürich who processed the GNSS data.

References

Aizen, V.B., Kuzmichenok, V.A., Surazakov, A.B., Aizen, E.M.: Glacier changes in the central and northern Tien Shan during the last 140 years based on surface and remote-sensing data, Annals of Glaciology, 43, 202-213, 2006.

Baltsavias, E.P., Favey, E., Bauder, A., Bösch H., Pateraki, M.: Digital surface modelling by airborne laser scanning and digital photogrammetry for glacier monitoring, Photogrammetric record, 17, 243-273, 2001.

Barrand, N.E., Murray, T., James, T.D., Barr, S.L., Mills, J.P.: Optimizing photogrammetric DEMs for glacier volume change assessment using laser-scanning derived ground-control points, Journal of Glaciology, 55, 106-116, 2009.

Benoit, L., Dehecq, A., Pham, H., Vernier, F., Trouvé, E., Moreau, L., Martin, O., Thom, C., Pierrot-Deseilligny, M., Briole, P.: Multi-method monitoring of Glacier d'Argentière dynamics, Annals of Glaciology, 56, 118-128, 2015.

Benoit, L., Gourdon, A., Vallat, R., Irarrazaval, I., Gravey, M., Lehmann, B., Prasicek, G., Gräff, D., Herman, F., Mariethoz, G.: A high-frequency and high-resolution image time series of the Gornergletscher - Swiss Alps - derived from repeated UAV surveys, doi: 10.5281/zenodo.1487862, 2018.

Berthier, E., Vincent, C., Magnússon, E., Gunnlaugsson, A., Pitte, P., Le Meur, E., Masiokas, M., Ruiz, L., Pálsson, F., Belart, J. M. C., Wagnon, P.: Glacier topography and elevation changes derived from Pléiades sub-meter stereo images, The Cryosphere, 8, 2275-2291, 2016a.

Berthier, E., Cabot, V., Vincent, C., Six, D.: Decadal Region-Wide and Glacier-Wide Mass Balances Derived from Multi-Temporal ASTER Satellite Digital Elevation Models. Validation over the Mont-Blanc Area, Frontiers in Earth Science, 4, 63, doi: 10.3389/feart.2016.00063, 2016b.

Brun, F., Wagnon, P., Berthier, E., Shea, J.M., Immerzeel, W.W., Kraaijenbrink, P.D.A., Vincent, C., Reverchon, C., Shrestha, D., Arnaud, Y.: Ice cliff contribution to the tongue-wide ablation ofChangri Nup Glacier, Nepal, central Himalaya, The Cryosphere, 12, 3439-3457, 2018.

Bhardwaj, A., Sam, L., Akanksha, Martín-Torres, F.J., Kumar, R.: UAVs as remote sensing platform in glaciology: Present applications and future prospects, Remote Sensing of Environment, 175, 196-204, 2016.

Chen, J., Funk, M.: Mass balance of Rhonegletscher during 1882/83–1986/87, Journal of Glaciology, 36, 199-209, 1990.

Chuang, M-C., Hwang, J-N., Williams, K., Towler, R.: Tracking Live Fish from Low-Contrast and Low-Frame-Rate Stereo Videos, IEEE Transactions on Circuits and Systems for Video Technology, 25(1), 167-179, 2015.

Cuffey, K. M., Paterson, W. S. B.: The physics of glaciers, Elsevier Science, 2010.

Dehecq, A., Gourmelen, N., Trouvé, E.: Deriving large-scale glacier velocities from a complete satellite archive: Application to the Pamir–Karakoram–Himalaya, Remote Sensing of Environment, 162, 55-66, 2015.

Dunse, T., Schuler, T.V., Hagen, J.O., Reijmer, C.H.: Seasonal speed-up of two outlet glaciers of Austfonna, Svalbard, inferred from continuous GPS measurements, The Cryosphere, 6, 453-466, 2012.

Fugazza, D., Scaioni, M., Corti, M., D'Agata, C., Azzoni, R.S., Cernuschi, M., Smiraglia, C., Diolaiuti, G.A.: Combination of UAV and terrestrial photogrammetry to assess rapid glacier evolution and map glacier hazards, Natural Hazards and Earth System Sciences, 18, 1055-1071, 2018.

Gabbud, C., Micheletti, N., Lane, S. N.: Lidar measurement of surface melt for a temperate Alpine glacier at the seasonal and hourly scales, Journal of Glaciology, 61, 963-974, 2015.

Gindraux, S., Boesch, R., Farinotti, D.: Accuracy assessment of digital surface models from Unmanned Aerial Vehicles' imagery on glaciers, Remote Sensing, 9, 186, doi: 10.3390/rs9020186, 2017.

Heid, T., Kääb A.: Evaluation of existing image matching methods for deriving glacier surface displacements globally from optical satellite imagery, Remote Sensing of Environment, 118, 339-355, 2012.

Herman, F., Anderson, B., Leprince, S.: Mountain glacier velocity variation during a retreat/advance cycle quantified using sub-pixel analysis of ASTER images, Journal of Glaciology, 57, 197-207, 2011.

Huss, M., Hock, R., Bauder, A., Funk, M.: Conventional versus reference-surface mass balance, Journal of Glaciology, 58, 278–286, 2012.

Immerzeel, W.W., Kraaijenbrink, P.D.A., Shea, J.M., Shrestha, A.B., Pellicciotti, F., Bierkens, M.F.P., de Jong, S.M.: High-resolution monitoring of Himalayan glacier dynamics using unmanned aerial vehicles, Remote Sensing of Environment, 150, 93-103, 2014.

James, M.R., Robson, S.: Mitigating systematic error in topographic models derived from UAV and ground-based image networks. Earth Surface Processes and Landforms, 39, 1413–1420, 2014.

Jouvet, G., Weidmann, Y., Seguinot, J., Funk, M., Abe, T., Sakakibara, D., Seddik, H., Sugiyama, S.: Initiation of a major calving event on the Bowdoin glacier captured by UAV photogrammetry, The Cryosphere, 11, 911-921, 2017.

Kääb, A., Berthier, E., Nuth, C., Gardelle, J., Arnaud, Y.: Contrasting patterns of early twenty-first-century glacier mass change in the Himalayas, Nature, 488, 495-498, 2012.

Kraaijenbrink, P., Meijer, S.W., Shea, J.M., Pellicciotti, F., De Jong, S.M., Immerzeel, W.W.: Seasonal surface velocities of a Himalayan glacier derived by automated correlation of unmanned aerial vehicle imagery, Annals of Glaciology, 57, 103-113, 2016.

Liu, B., Zaccarin, A.: New Fast Algorithms for the Estimation of Block Motion Vectors, IEEE Transactions on Circuits and Systems for Video Technology, 3(2), 148-157, 1993.

Maksymiuk, O., Mayer, C., Stilla, U.: Velocity estimation of glaciers with physically-based spatial regularization - Experiments using satellite SAR intensity images, Remote Sensing of Environment, 172, 190-204, 2016.

Mertes, J.R., Gulley, J.D., Benn, D.I., Thompson, S.S., Nicholson, L.I.: Using structure-from-motion to create glacier DEMs and orthoimagery from historical terrestrial and oblique aerial imagery, Earth Surface Processes and Landforms, 42, 2350-2364, 2017.

Piermattei, L., Carturan, L., Guarnieri, A.: Use of terrestrial photogrammetry based on structure-from-motion for mass balance estimation of a small glacier in the Italian alps, Earth Surface Processes and Landforms, 40, 1791-1802, 2015.

Racoviteanu, A., Williams, M.W.: Decision tree and texture analysis for mapping debris-covered glaciers in the Kangchenjunga area, Eastern Himalaya, Remote Sensing, 4, 3078-3109, 2012.

Ramirez, E., Francou, B., Ribstein, P., Descloitres, M., Guérin, R., Mendoza, J., Gallaire, R., Pouyaud, B., Jordan, E.: Small glaciers disappearing in the tropical Andes: a case-study in Bolivia: Glaciar Chacaltaya (16° S), Journal of Glaciology, 47, 187-194, 2001.

Riesen, P., Sugiyama, S., Funk, M.: The influence of the presence and drainage of an ice-marginal lake on the flow of Gornergletscher, Switzerland, Journal of Glaciology, 56, 278-286, 2010.

Rippin, D.M., Pomfret, A., King, N.: High resolution mapping of supra-glacial drainage pathways reveals link between micro-channel drainage density, surface roughness and surface reflectance, Earth Surface Processes and Landforms, 40, 1279-1290, 2015.

Rossini, M., Di Mauro, B., Garzonio, R., Baccolo, G., Cavallini, G., Mattavelli, M., De Amicis, M., Colombo R.: Rapid melting dynamics of an alpine glacier with repeated UAV photogrammetry, Geomorphology, 304, 159-172, 2018.

Ryan, J.C., Hubbard, A.L., Box, J.E., Todd, J., Christoffersen, P., Carr, J.R., Holt, T.O., Snooke, N.: UAV photogrammetry and structure from motion to assess calving dynamics at Store Glacier, a large outlet draining the Greenland ice sheet, The Cryosphere, 9, 1-11, 2015.

Scherler, D., Leprince, S., Strecker, M.R.: Glacier-surface velocities in alpine terrain from optical satellite imagery—Accuracy improvement and quality assessment, Remote Sensing of Environment, 112, 3806-3819, 2008.

Sold, L., Huss, M., Machguth, H., Joerg, P. C., Leysinger Vieli, G., Linsbauer, A., Salzmann, N., Zemp, M.,Hoelzle, M.: Mass balance re-analysis of Findelengletscher, Switzerland; benefits of extensive snow accumulation measurements, Frontiers in Earth Science, 4, doi: 10.3389/feart.2016.00018, 2016.

Sugiyama, S., Bauder, A., Riesen, P., Funk, M.: Surface ice motion deviating toward the margins during speed-up events at Gornergletscher, Switzerland, Journal of Geophysical Research: Earth Surface, 115, doi: 10.1029/2009JF001509, 2010.

Vallet, J., Panissod, F., Strecha, C., Tracol, M.: Photogrammetric performance of an ultra light weight swinglet 'UAV', International Archives of the Photogrammetry, Remote Sensing and Spatial Information Sciences, XXXVIII-1, 253-258, 2011.

Werder, M. A., Loye, A., Funk, M.: Dye tracing a jökulhlaup : I. subglacial water transit speed and water-storage mechanism, Journal of Glaciology, 55, 889–898, 2009.

Werder, M. A., Funk, M.: Dye tracing a jökulhlaup : II. Testing a jökulhlaup model against flow speeds inferred from measurements, Journal of Glaciology, 55, 899-908, 2009.

Werder, M.A., Hewitt, I.J., Schoof, C.G., Flowers, G.E.: Modeling channelized and distributed subglacial drainage in two dimensions, Journal of Geophysical Research: Earth Surface, 118, 2140-2158, 2013.

Whitehead, K., Moorman, B.J., Hugenholz, C.H.: Brief Communication: Low-cost, on-demand aerial photogrammetry for glaciological measurement, The Cryosphere, 7, 1879-1884, 2013.

Yang, K., Smith, L.C.: Supraglacial Streams on the Greenland Ice Sheet Delineated From Combined Spectral–Shape Information in High-Resolution Satellite Imagery, IEEE Geoscience and Remote Sensing Letters, 10, 801-805, 2012.